Properties of Uranium-Zirconium Hydride Moderated Nuclear Fuel Synthesized by Powder Metallurgy

Caitlin Taylor, Tyler Smith, Michael Hahn, James Torres, Eric Tegtmeier, Thomas Nizolek, Kevin Bohn, Conor Emberley, Aditya Shivprasad, Scarlett Widgeon-Paisner, Adrien Terricabras, Erik Luther

Executive Summary

Prepared for: U.S. Department of Energy/National Nuclear Security Administration, Los Alamos Field Office

Prepared by: **Caitlin Taylor**, Scientist 3
MST-8

1   Introduction

Applications of uranium-zirconium hydride (U-ZrH$_x$) as a nuclear fuel or ZrH$_x$ as a moderator for nuclear reactors goes back nearly as far as oxide fuels. The fuel was initially fabricated for the Space Nuclear Auxiliary Power (SNAP) in the 1960s [1-3]. These early hydride fuels used highly enriched U or U-235 of various enrichment levels. Metal hydrides contain high densities of hydrogen which effectively slow neutrons into the thermal energy regime and increases the probability of fission. This higher fission efficiency allows for smaller reactor designs and lower U-235 enrichment. General atomics currently manufactures U-ZrH$_x$ for their Training, Research, Isotopes, General Atomics (TRIGA) research reactors. TRIGA fuel was developed around the concept of inherent safety [4]. General Atomics sought a core composition that had a large prompt negative temperature coefficient of reactivity such that if all the available excess reactivity were suddenly inserted into the core, the resulting fuel temperature would automatically cause the power excursion to terminate before any core damage resulted. The DOE Microreactor Program has investigated fabrication procedures and properties of U-ZrH$_x$ fuel for use in demonstration reactors, which was the purpose of this work. A thorough understanding of the fuel and moderator phase space and properties under reactor operating conditions is necessary for predicting performance. The Zr-H and U-Zr-H systems are both eutectoids. The zirconium-hydrogen system (Fig 1) exhibits several equilibrium phases, including hydrogen-infused metallic hexagonal α-phase at low temperature, hydrogen-infused metallic body-centered cubic (bcc) β-phase at high temperature, hydride face-centered cubic (fcc) δ-phase, and hydride body-centered tetragonal (bct)

Figure 1. Zirconium-hydrogen phase diagram. Insets are drawings of each crystal structure. Densities used to calculate the volume expansion between phases are listed.

ε-phase [5]. The ε-phase is not a true equilibrium phase and forms from the δ-phase by a martensitic reaction. It appears as a banded twin structure. When uranium is present, it appears to be partially rejected from solution during the hydriding process. The effect of adding uranium to the Zr-H system is to shift all the phase boundaries of the Zr-H diagram to slightly lower temperatures (the eutectoid temperature is lowered from 547 to 541°C) [4, 6]. At high uranium contents (25-50 wt.%), hydrogen causes partitioning of the UZr alloy. Zirconium reacts with the hydrogen, giving polyphase regions of uranium, zirconium, and zirconium hydride phases. The phase boundaries in the Zr-H system are relatively unaffected in the region of high hydrogen content, but the α- and β-phases are markedly shifted in U-ZrH. Primarily, uranium considerably increases the range of the α-phase. TRIGA reactor fuel has a hydrogen-to-metal ratio (H/M) of 1.6 (δ-phase), SNAP designs used H/M = 1.68-1.83 (ranging from δ- to ε-phase), and the MARVEL reactor is expected to use H/M = 1.7 (δ+ε-phases). Different reactor designs also vary in the U/ZrH$_x$ ratio.

Fabrication of hydride fuel presents a challenging problem due to the high volume expansion induced by the Zr hydriding reaction (14% from α to δ, 19% from β to δ, and an additional 2% from δ to ε). The hydriding reaction must be carefully controlled to prevent cracking during the volume expansion. Traditional methods use arc-melting to form U-Zr alloy followed by hydriding in a Sieverts-type apparatus to limit reaction rates using small aliquots of hydrogen [7], or hydriding in a furnace containing a controlled volume of hydrogen [8]. In this work, we developed a powder metallurgy method for fabricating U-ZrH$_x$. This method allows for fabrication without arc-melting and provides some internal porosity which might help relieve stresses during hydriding. U-ZrH$_x$ samples were characterized to determine H/M, crystallographic phase, microstructure, thermophysical properties, hydrogen release, and elastic properties.

2   Materials and Methods

The first step in powder metallurgy (PM) fabrication entails producing ZrH_x and UH_3 powder by direct hydriding machined metal pieces. High purity crystal bar Zr (ATI Inc) and U metal were used for this work. ZrH_x powder is then ground using a SPEX mill and mortar and pestle inside an Ar atmosphere glovebox to prevent oxidation. UH_3 pulverizes into fine powder during hydriding. ZrH_x powder is sieved to 200 mesh (75 μm) and UH_3 powder is sieved through 325 mesh (44 μm) to control the maximum particle size. After sieving, powders are weighed and mixed into a 40 wt.% UH_3 mixture using a SPEX mill for 10-15 min. The powder is then pressed into pellets using 250 MPa. These data were collected on pellets prepared from

$ZrH_{1.7}$ feedstock powder. Data are not currently available on how the initial powder phase and stoichiometry might affect the final pellet. Green pellets are placed on a molybdenum sheet and covered with pure zirconium crucibles which act as internal oxygen getters. The sample boat is quickly transferred from the argon glovebox into a tube furnace, sealed and flushed with high purity argon. Argon gas is taken from a dewar and purified using a Centorr copper getter. The furnace run consists of a 1400°C sintering step in argon gas followed by a series of hydriding steps in flowing 6% H_2/ Ar gas. Though pellets are prepared from hydride powder, most of the hydrogen desorbs during sintering and must be re-absorbed through subsequent hydriding

Figure 2. Zirconium-hydrogen phase diagram (black) overlayed with PCT curves from the literature (rainbow).

steps. The 6% H_2/ Ar gas is taken from a cylinder without gettering. The hydriding profile was developed by referencing published pressure-composition-temperature (PCT) data [5], shown in Fig 2. Though others have measured PCT curves in a 45 wt.% U-Zr system, the changes mostly appear to occur in the 2-phase region and do not significantly change the hydriding profile [7]. The profile was optimized to maximize absorption at higher temperatures where hydrogen diffusion rates are higher. Published hydrogen diffusivity values show slow diffusion in α-Zr [9] and δ-ZrH_x [10-13], but fast diffusion in β-Zr [14]. Figure 3 shows the as-fabricated samples. The gold color indicates possible formation of a nitride layer at the surface (typically <1 μm in thickness). Samples are typically approximately 64% theoretical density (TD) as green pellets and 95% TD after the furnace run. The ZrH_x TD is determined using an expression developed by Simnad for density as a function of H/M [6], given below in g/cm³.

$$\rho_{ZrH} (\text{g·cm}^{-3}) = 1/(0.1541 + 0.0145\, x) \text{ for } x < 1.6$$

$$\rho_{ZrH} (\text{g·cm}^{-3}) = 1/(0.1706 + 0.0042\, x) \text{ for } x \geq 1.6$$

Rule of mixtures is then used to approximate the TD of the 40 wt.% U hydride fuel, where w_U and w_{ZrH} are the weight fraction of uranium and zirconium hydride, respectively, and ρ_U is the uranium density (taken to be 19.1 g/cm³).

$$\rho_{UZrH} (\text{g·cm}^{-3}) = 1/(w_U/\rho_U + w_{ZrH}/\rho_{ZrH})$$

Samples are first characterized to determine hydrogen stoichiometry. Stoichiometry is typically determined in hydrides by measuring the weight before and after hydriding and attributing all weight gain to hydrogen. This method cannot be accurately performed on powder metallurgy samples because the green pellets are made with hydride powders and there is too little weight change. Machined Zr witness samples are therefore often placed in the furnace runs so that H/M can be approximated by weight. Machined samples are 100% dense and different sizes from the powder metallurgy samples so the H/M is not always representative of the fuel. Representative PM samples from each run are sent for LECO elemental analysis to determine the H/M. Duplicate or triplicate LECO samples are measured from different parts of the bulk sample. Since LECO is a destructive analysis method, not all samples can be tested using this procedure; therefore, all powder metallurgy samples in the furnace run are assumed to have the same H/M as the LECO sample. It is recognized that LECO measurements are an imperfect measurement method because hydrogen is rapidly released from the sample which can saturate the detector and lead to incorrect H/M measurements. However, the method has been demonstrated to be a good guide and additional refinement of the procedure is being investigated. Currently, the measurement utilizes small pieces (0.01-0.03 g) taken from a larger sample to minimize detector saturation but which can lead to measurement inaccuracies or sampling errors. XRD was measured on a representative powder metallurgy sample to determine the phases present. The sample was ground into powder in an argon glovebox and fixed to an inert-atmosphere sample holder with a slit. A Bruker D2 phaser was used for the XRD measurements. In some cases, XRD data were collected from the surface of pellets to make non-destructive measurements. Samples were characterized with scanning electron microscopy (SEM), energy dispersive x-ray spectroscopy (EDS), and optical microscopy.

Figure 3. 40%U-ZrH$_x$ pellets fabricated by powder metallurgy. Samples were fabricated in dimensions required for thermophysical property measurements.

Hydrogen release measurements were performed using a Netzsch simultaneous thermal analyzer (STA) Model 449 F3 Jupiter. This analysis method measures the mass changes from thermal effects. The mass loss in these samples during the temperature ramp is assumed to be hydrogen release. The samples were heated to approximately 1000°C at a ramp rate of 1°C/min under an argon purge gas and mass was recorded every 4 seconds. Note that the rates of hydriding and dehydriding could be influenced by the presence of surface oxide or nitride films [4]. The thermal diffusivity measurements were acquired using a Netzsch Light Flash Apparatus (LFA) Model 467 HyperFlash. The U-ZrH$_x$ samples were carbon-coated prior to measurement exposure using (carbon spray). The thermal diffusivity, α, of the samples was recorded in the temperature ranges of 25-600°C at 25°C increments using the laser-flash analysis method (LFA). Each measurement was performed three times. The samples were only measured up to 600°C to avoid decomposition at high temperatures. The specific heat capacity, C_p, was measured by dynamic scanning calorimetry (DSC) using a Netzsch DSC Model 404 F1 Pegasus. The samples were calibrated using a sapphire disc, and placed in an alumina-lined platinum crucible, and covered with a platinum top cap. An argon cover gas was

Figure 4. Bright field optical image of an as-fabricated 40%U-ZrH$_x$ pellet cross-section.

flowed into the measurement chamber to prevent oxidation during heat capacity measurements. Heat capacity measurements were acquired in the temperature ranges of 25-600°C in 5°C increments. Thermal conductivity, λ, was calculated from the thermal diffusivity, heat capacity, and density of the samples using the expression $\lambda = \alpha C_p \rho$. Elongation and the coefficient of thermal expansion (CTE) for these samples were measured using a NETZCH DIL 402 temperature-dependent dilatometer, capable of ±2 nm precision over the temperature range of 41-1051°C. The samples were calibrated with an alumina (Al$_2$O$_3$) standard and heated to approximately 600°C at a ramp rate of 1.5°C/min under an argon purge gas.
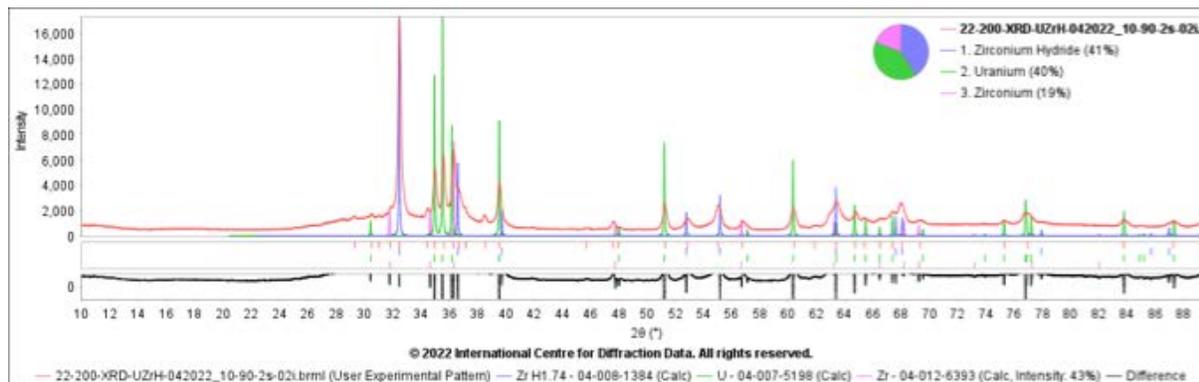
Figure 5. XRD results from as-fabricated 40%U-ZrH$_{1.6}$ pellet.

3   Results and Discussion

3.1   Stoichiometry, Phase and Microstructure

Samples were high density with no visible cracking, as shown in an optical cross-section image in Fig 4. LECO measurements of a representative sample showed H/M of 1.6. (A Zr witness sample placed in the same furnace run had a H/M of 1.7 by weight.) Remnants from the same sample were pulverized and used for powder XRD, shown in Fig 5. The XRD showed primarily metallic uranium and ε-phase zirconium hydride, with a small amount of unconverted zirconium metal. The pure ε-phase zirconium hydride boundary occurs at H/M~1.7. This suggests that the LECO results are somewhat low, or that ε-phase is stabilized at lower H/M in the U-ZrH$_x$ composite.

Fig 6 shows a backscattered electron (BSE) SEM image and EDS map of the resulting microstructure. In the backscatter SEM images, uranium appears white and zirconium hydride appears dark. During the ramp to sintering temperature the hydride phases are expected to decompose to metal under the hydrogen partial pressure of zero. Upon reaching the sintering temperature of 1400°C, uranium and some of the zirconium are expected to form an intermetallic. Some zirconium is expected to remain unreacted. The matrix of the microstructure appears to suggest melting of a uranium-zirconium intermetallic, which then segregated into uranium metal and zirconium hydride upon
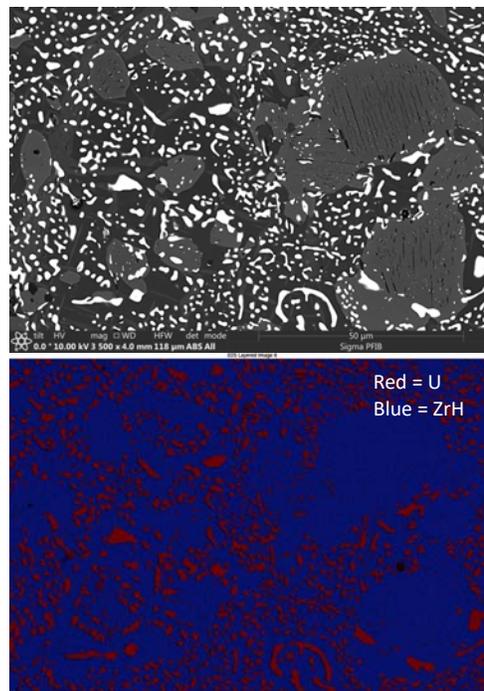
Figure 6. (left) BSE SEM image and (right) EDS of an as-fabricated 40%U-ZrH$_{1.6}$ sample.

hydriding. Large grains of unreacted zirconium hydride are also present. Fig 7 shows a comparison of a pure zirconium hydride sample, fabricated from just $ZrH_{1.7}$ powder in the same furnace run, and a 40% U-$ZrH_{1.6}$ sample. The pure zirconium hydride sample contains large, fully twinned grains, as expected in ε-ZrH [15]. In this case the H/M of the pure ZrH_x sample was not measured by LECO but is assumed close to the witness sample which had H/M = 1.7. Uranium precipitates appear along the possible twin boundaries, which would have occurred during sintering and convolutes the microstructure compared to a pure ε-phase zirconium hydride sample.
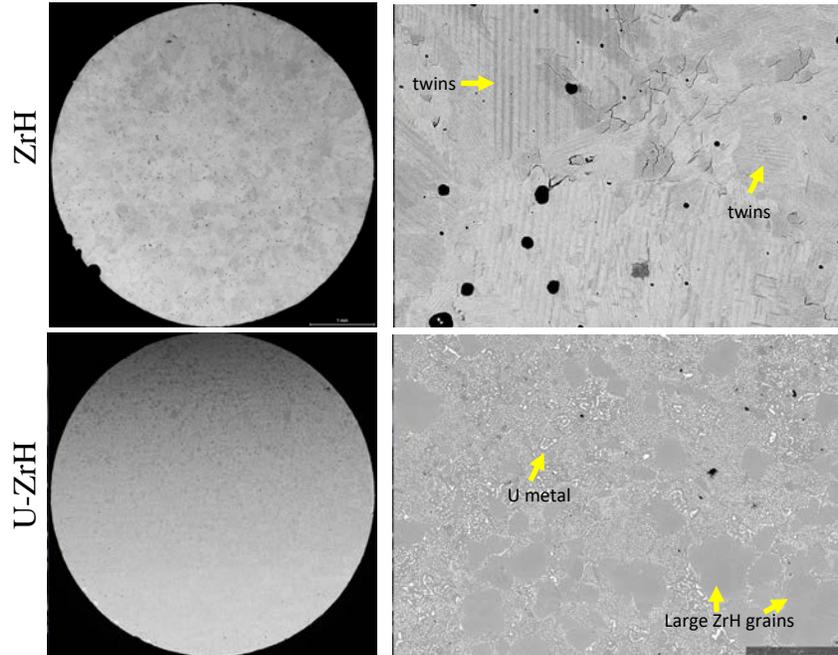
Figure 7. BSE SEM images comparing pure ZrHx and 40 wt.% U-$ZrH_{1.6}$ samples fabricated in the same furnace run. Arrows point to regions where 1) ε-ZrH appears to present the typical twinned microstructure; 2) U-metal appears, and 3) large ZrH grains appear.

3.2   Hydrogen Release Measurements

STA measurements recorded mass loss due to hydrogen release from 40% U-ZrH1.6 during heating. The data were converted to H/M using the initial H/M of 1.6 obtained by LECO, shown in Fig 8. The approximate phases at each stage of hydrogen release were predicted using the equilibrium Zr-H phase diagram in Fig 1. This is an approximation because Fig 2 shows that the hydride phase is not in equilibrium when the H_2 partial pressure is zero, so hydrogen release is based solely on kinetics. The initial region is labeled ε+δ because the phase diagram suggests the sample starts in δ-phase but the XRD measurements show the sample starts in ε-phase, so the phase boundaries in this system are not perfectly understood. Hydrogen release occurred starting at 670°C, in general agreement with General Atomics results where release occurred at 650°C [6]. Complete hydrogen loss occurs by 900°C. The sample exhibited linear hydrogen loss between 750 and 900°C. A fit of this region provides an expression for H/M as a function of temperature, given below.

$$H/M = -0.0096 \times T(°C) + 8.5915$$
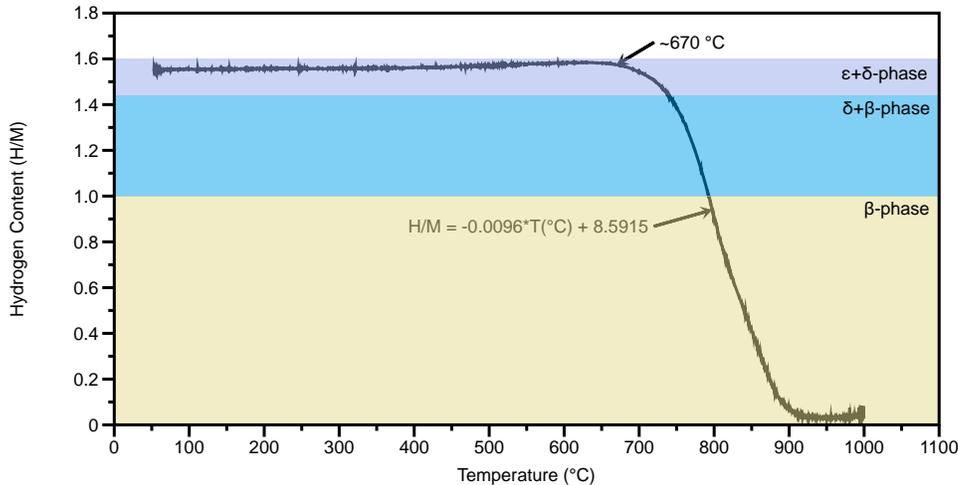
Figure 8. STA curve showing hydrogen release from a 40%U-ZrH$_{1.6}$ sample. Inset equation provides an expression for hydrogen loss. Colored regions show approximate phases at different stages of hydrogen release.

3.3   Thermal Diffusivity

Measured thermal diffusivity of 40% U-ZrH$_{1.6}$ is shown in Fig 9. No variation in the data occurred between ramp up and ramp down, indicating no hydrogen loss during heating. Fig 9 shows a comparison of these data with the Kakiuchi 45% U-Zr alloy and 45% U-ZrH$_{1.6}$ data [7]. The Kakiuchi 45% U-ZrH$_{1.6}$ results are slightly lower than this work, but in general good agreement given the different uranium weight fractions, the difficulty in measuring a precise H/M, and hydrogen homogeneity in the composite. Above 600°C the Kakiuchi 45% U-ZrH$_{1.6}$ data begin to agree with the 45% U-Zr data, indicating hydrogen loss. Data from this work were fit with a 2nd order polynomial to obtain the expression below.

$$\alpha \ (\text{mm}^2/\text{s}) = 10.72 - 0.0112 \times T(°C) + 8.1 \times 10^{-6} T(°C)^2$$
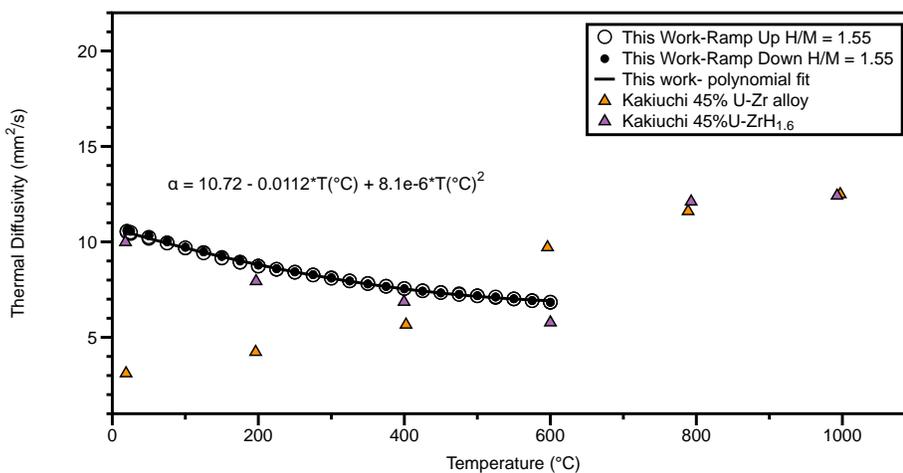
Figure 9. Thermal diffusivity data from this work (40% U-ZrH$_{1.6}$) and Kakiuchi (45% U-ZrH$_{1.6}$).

3.4   Specific Heat Capacity

Measured specific capacity data are given in Fig 10. The data show three distinct regions, including an initial linear region from 0-220°C, a steep drop from 220-280°C, and a mostly linear region with a bit of curvature at 375°C from 280-600°C. The physical phenomena behind the regions of curvature in these data are unknown. The behavior was reversible on cooling, and the temperature was low enough to prevent hydrogen loss, so any phase transformation would need to be reversible. One possibility is that this sample underwent a reversible phase transformation from δ+ε to pure δ upon heating to 220°C. Kakiuchi data [7] match this work until the drop in heat capacity at 220°C, where the Kakiuchi data continue a linear trend but undergo a similar drop in heat capacity at around 375°C. Both datasets show much higher heat capacity in the hydride as opposed to the pure alloy. The average specific heat capacity was fit with several curves describing the specific heat capacity in each temperature range. Those expressions are given below.

$$C_p(0 - 220°C) = 0.24413 + 0.00051627 \times T(°C)$$

$$C_p(220 - 280°C) = -7.26102 + 0.09198356 \times T(°C) - 0.0003682338 \times T(°C)^2 + 4.88792 \times 10^{-7} \times T(°C)^3$$

$$C_p(280 - 600°C) = 4.1958 - 0.0483017 \times T(°C) + 0.000234226 \times T(°C)^2 - 5.502403 \times 10^{-7} \times T(°C)^3$$
$$+ 6.32871 \times 10^{-10} \times T(°C)^4 - 2.85767 \times 10^{-13} \times T(°C)^5$$
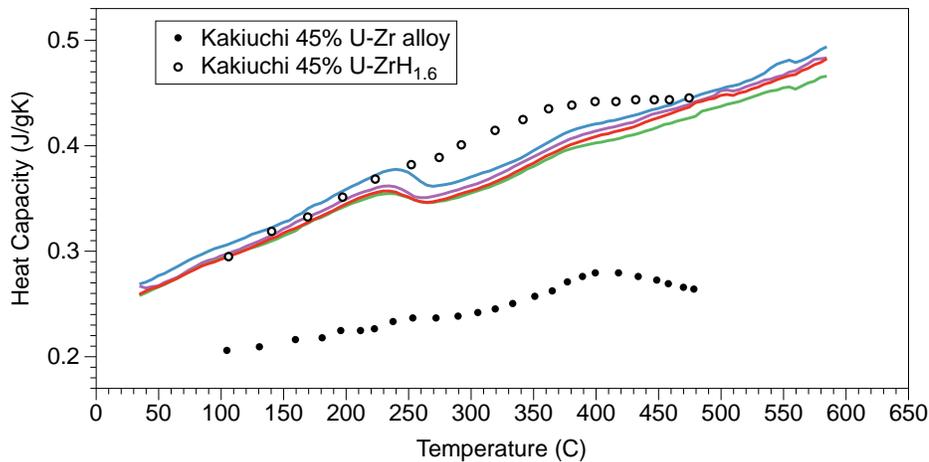
Figure 10. Specific heat capacity of 40% U-ZrH$_{1.6}$. Data collected in this work are shown in colored lines, one line per measurement. Kakiuchi data on 45% U-Zr alloy and hydride are shown as points.

3.5   Thermal Conductivity

Thermal conductivity calculated from the measured thermal diffusivity and heat capacity is shown in Fig 11. Again, the thermal conductivity of 40% U-ZrH$_{1.6}$ used in this work agrees well with the Kakiuchi data [7] on 45% U-ZrH$_{1.6}$ until about 220°C. Thermal conductivity of the hydride is much higher than the 45% U-Zr alloy measured by Kakiuchi.
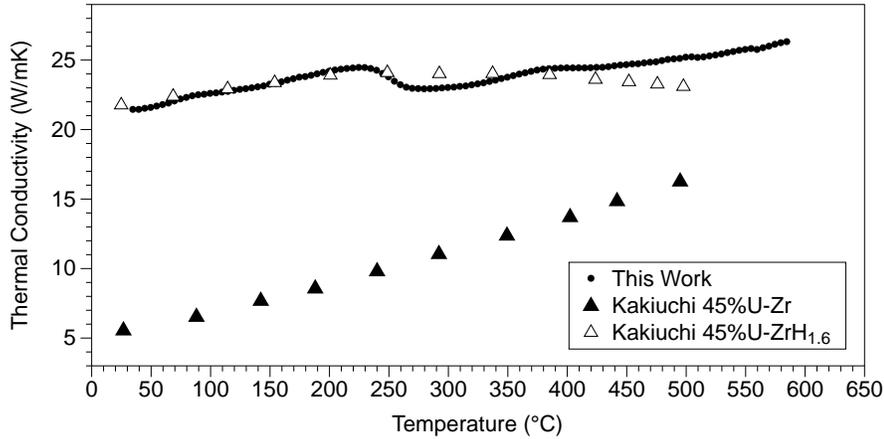
Figure 11. Thermal conductivity of 40% U-ZrH$_{1.6}$. Kakiuchi data on 45% U-Zr alloy and hydride are shown.

3.6   Thermal Expansion

Dilatometry data on the 40% U-ZrH$_{1.6}$ are shown in Fig 12. Hydrogen desorption occurred at 640°C during this measurement, which was collected using a slightly higher ramp rate than the STA data. This reasonably agrees with the point where hydrogen release first occurred in the STA data (670°C). Coefficient of thermal expansion was calculated by performing a linear fit of $\Delta l/l_o$ as a function of T. Only data up to 640°C were used in the fit, which is given below. To the best of our knowledge, no other thermal expansion data is available on U-ZrH$_x$ in the literature.

$$\Delta l/l_o = -9.6016 \times 10^{-4} + 1.0049 \times 10^{-5} \times T(°C)$$
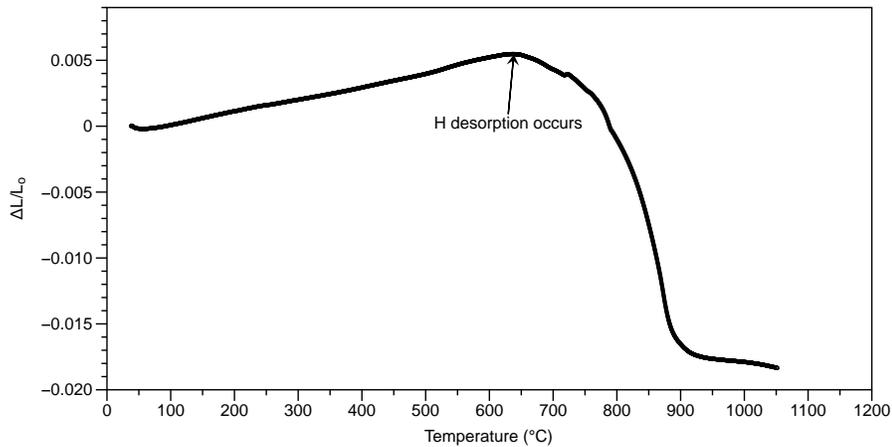
Figure 12. Dilatometry data collected from 40% U-ZrH$_{1.6}$. Hydrogen desorption occurs at 640°C.

4   Conclusions

Powder metallurgy was used to fabricate crack-free >95% dense 40 wt.% U-ZrH$_x$ pellets. LECO analysis showed H/M = 1.6, but XRD results showed the presence of ε-ZrH$_x$, which usually occurs at H/M > 1.7. This indicates that the LECO results may be artificially low, or that ε-phase is stabilized at lower H/M in

the U-ZrH$_x$ composite. Microstructural characterization appears to show liquid phase sintering of a uranium-zirconium intermetallic, with phase segregation occurring during hydriding. Large unreacted zirconium-hydride grains were present. Microscopy showed structures similar to twins in these large grains, but it remains unclear whether these features formed during fabrication of the feedstock powder or during the final sinter-hydride furnace run. STA measurements showed hydrogen release at 670°C, in agreement with the literature. Release occurred linearly with temperature from that point until 900°C when the sample had fully desorbed. Thermal diffusivity data closely matched the literature. Heat capacity data matched the literature until 220°C, where a sharp drop occurred in our data with an unknown cause. Thermal conductivity was calculated from the measured thermal diffusivity and heat capacity, so it showed the same trend with relation to literature. The coefficient of thermal expansion was measured for 40 wt.% U-ZrH$_{1.6}$ and fit to a curve. Overall, this work shows that powder metallurgy is a highly effective method for producing high-density crack-free U-ZrHx, Properties were compared to the study by Kakiuchi *et al* [7], where they fabricated 45% U-ZrH$_{1.6}$ by arc-melting and subsequent hydrogenation in a Sievert's apparatus. Hydrogen release data agreed reasonably well with General Atomics data, which was also collected on samples produced by arc-melting [6]. Thermophysical properties and microstructure agreed reasonably well between samples fabricated through powder metallurgy and arc-melting.

5   Acknowledgements

6   References

[1] D.R. Olander, M. Ng, Hydride fuel behavior in LWRs, Journal of Nuclear Materials 346 (2005) 98-108.

[2] D. Olander, K. Konashi, M. Yamawaki, Uranium-Zirconium Hydride Fuel, Elseveir Ltd.2012.

[3] D. Olander, E. Greenspan, H.D. Garkisch, B. Petrovic, Uranium-zirconium hydride fuel properties, Nuclear Engineering and Design 239 (2009) 1406-1424.

[4] M.T. Simnad, F.C. Foushee, G.B. West, Fuel elements for pulsed TRIGA research reactors, Nuclear Technology 28(1) (1976) 31-56.

[5] E. Zuzek, J.P. Abriata, A. San-Martin, F.D. Manchester, The H-Zr (Hydrogen-Zirconium) System, Bulletin of Alloy Phase Diagrams 11(4) (1990) 385-395.

[6] M.T. Simnad, The U-ZrHx alloy: its properties and use in TRIGA fuel, Nuclear Engineering and Design 64 (1981) 403-422.

[7] K. Kakiuchi, N. Itagaki, T. Furuya, T. Hattori, Y. Nakazono, F. Ono, K. Yamaguchi, M. Yamawaki, Thermal properties of hydride fuel 45% U-ZrH1.6, Journal of Nuclear Materials 294 (2001) 28-31.

[8] U. Merten, L.J. Dijkstra, F.D. Carpenter, A.P. Hatcher, L.D. La grange, The Preparation and Properties of Zirconium-Uranium-Hydrogen Alloys, Proceedings of the Second United Nations International Conference ont he Peaceful Uses of Atomic Energy 6 (1958) 111-115.

[9] E.A. Gulbransen, K.F. Andrew, Diffusion of hydrogen and deuterium in high purity zirconium, Journal of the Electrochemical Society 101 (1954).

[10] H. Wipf, B. Kappesser, R. Werner, Hydrogen Diffusion in Titanium and Zirconium Hydrides, Journal of Alloys and Compounds 310 (2000) 190-195.

[11] C. Korn, S.D. Goren, NMR Study of Hydrogen Diffusion in Zirconium Hydride, Physical Review B 33(1) (1968) 68-78.

[12] G. Majer, W. Renz, R.G. Barnes, The mechanism of hydrogen diffusion in zirconium dihydrides, Journal of Physics: Condensed Matter 6 (1994) 2935-2942.

[13] S.D. Harkness, W.A. Young, Diffusion Coefficient of Hydrogen in Delta-Phase Zirconium Hydride, (1965).

[14] V.L. Gelezunas, P.K. Conn, R.H. Price, The Diffusion Coefficients for Hydrogen in beta-Zirconium, Journal of the Electrochemical Society 110 (1963).

[15] H. Muta, R. Nishikane, Y. Ando, J. Matsunaga, K. Sakamoto, S. Harjo, T. Kawasaki, Y. Ohishi, K. Kurosaki, S. Yamanaka, Effect of hydrogenation conditions on the microstructure and mechanical properties of zirconium hydride, Journal of Nuclear Materials 500 (2018) 145-152.